Neurobiology of Disease 96 (2016) 323–334

Contents lists available at ScienceDirect

Neurobiology of Disease

journal homepage: www.elsevier.com/locate/ynbdi

N-acetylaspartate supports the energetic demands of developmental myelination via oligodendroglial aspartoacylase

Jeremy S. Francis, PhD [a], Ireneusz Wojtas, PhD [a], Vladimir Markov, MD [a], Steven J. Gray, PhD [b], Thomas J. McCown, PhD [c], R. Jude Samulski, PhD [d], Larissa T. Bilaniuk, MD [e], Dah-Jyuu Wang, PhD [e], Darryl C. De Vivo, MD [f], Christopher G. Janson, MD [g], Paola Leone, PhD [a,*]

[a] Department of Cell Biology, Cell & Gene Therapy Center, Rowan School of Osteopathic Medicine, Stratford, NJ, USA
[b] Department of Ophthalmology, UNC, Chapel Hill, NC, USA
[c] Department of Psychiatry, UNC, Chapel Hill, NC, USA
[d] Department of Pharmacology and Gene Therapy Center, UNC, Chapel Hill, NC, USA
[e] Department of Radiology, Children's Hospital of Philadelphia, Philadelphia, PA, USA
[f] Department of Neurology, Columbia University, NY, USA
[g] Department of Neurology & Rehabilitation, University of Illinois at Chicago, Chicago, USA

ARTICLE INFO

Article history:
Received 30 August 2016
Revised 27 September 2016
Accepted 1 October 2016
Available online 04 October 2016

Keywords:
N-acetylaspartate
Aspartoacylase
Canavan disease
Myelination
Energy

ABSTRACT

Breakdown of neuro-glial *N*-acetyl-aspartate (NAA) metabolism results in the failure of developmental myelination, manifest in the congenital pediatric leukodystrophy Canavan disease caused by mutations to the sole NAA catabolizing enzyme aspartoacylase. Canavan disease is a major point of focus for efforts to define NAA function, with available evidence suggesting NAA serves as an acetyl donor for fatty acid synthesis during myelination. Elevated NAA is a diagnostic hallmark of Canavan disease, which contrasts with a broad spectrum of alternative neurodegenerative contexts in which levels of NAA are inversely proportional to pathological progression. Recently generated data in the nur7 mouse model of Canavan disease suggests loss of aspartoacylase function results in compromised energetic integrity prior to oligodendrocyte death, abnormalities in myelin content, spongiform degeneration, and motor deficit. The present study utilized a next-generation "oligotropic" adeno-associated virus vector (AAV-Olig001) to quantitatively assess the impact of aspartoacylase reconstitution on developmental myelination. AAV-Olig001-aspartoacylase promoted normalization of NAA, increased bioavailable acetyl-CoA, and restored energetic balance within a window of postnatal development preceding gross histopathology and deteriorating motor function. Long-term effects included increased oligodendrocyte numbers, a global increase in myelination, reversal of vacuolation, and rescue of motor function. Effects on brain energy observed following AAV-Olig001-aspartoacylase gene therapy are shown to be consistent with a metabolic profile observed in mild cases of Canavan disease, implicating NAA in the maintenance of energetic integrity during myelination via oligodendroglial aspartoacylase.

1. Introduction

Canavan disease is an autosomal recessive leukodystrophy caused by deficiency in aspartoacylase (ASPA) (Hagenfeldt et al., 1987), an oligodendroglial enzyme (Baslow et al., 1999) (Madhavarao et al., 2004) (Dugas et al., 2006) (Francis et al., 2011) (Zhang et al., 2014) that catabolizes *N*-acetyl-aspartate (NAA). NAA has multiple hypothesized functions as an osmolyte (Baslow, 2003; Taylor et al., 1995), a building block for myelin synthesis (Chakraborty et al., 2001; Madhavarao et al., 2005; Mehta and Namboodiri, 1995), a metabolic intermediate (D'Adamo and D'Adamo, 1968) (Mehta and Namboodiri, 1995), and developmental signal molecule (Francis et al., 2006). Based on these diverse roles, it follows that the effects of dysregulated NAA in Canavan disease are likely multi-factorial. Given the genetic defect underlying Canavan disease is manifest primarily in the oligodendroglial compartment, targeting of this specific lineage is required to address the relative prominence of these multifactorial effects and provide insight into pathogenic mechanisms of relevance to clinical endpoints.

NAA rises linearly with age in Canavan disease (Janson et al., 2006b; Leone et al., 2012) alongside progressive spongiform encephalopathy and diffuse white matter loss. Mitochondrial dysfunction has long been suspected based on ultrastructural studies (Gambetti et al., 1969), and a relatively unexplored role for NAA in uncoupling the

* Corresponding author at: Cell & Gene Therapy Center, RowanSOM, 2 Medical Center Drive, Stratford, NJ 08084, USA.
E-mail address: leonepa@rowan.edu (P. Leone).
Available online on ScienceDirect (www.sciencedirect.com).

http://dx.doi.org/10.1016/j.nbd.2016.10.001
0969-9961/

Krebs cycle from myelin lipid synthesis has recently come into focus (Francis et al., 2014). NAA synthesis is an energy-intensive process that is tightly coupled to mitochondria derived substrate (Bates et al., 1996). Consequently, reductions in NAA are regarded as a marker of compromised energetic integrity across the neurodegenerative spectrum, with the notable exception of Canavan disease. Canavan disease, in contrast to disorders such as Alzheimer's disease (Huang et al., 2001), multiple sclerosis (De Stefano et al., 2001), and Huntington's disease (Sturrock et al., 2010), is the sole brain disorder in which increases in brain NAA are considered pathological.

Clinical gene therapy trials have been undertaken with the aim of lowering pathologically elevated NAA (Janson et al., 2002; Leone et al., 2000; Leone et al., 2012). These trials employed technology limited in tropism, not capable of targeting oligodendroglia. While neurotropic delivery of ASPA was successful in broadly lowering NAA, this was insufficient to maintain normal myelination or true reversal of phenotype (Leone et al., 2012). Because ASPA naturally occurs in oligodendrocytes, it is possible that neurotropic intervention failed to address pathological endpoints of specific relevance to white matter producing cells. The availability of animal models for Canavan disease lagged behind human experimentation, resulting in gaps in our knowledge of the nature of the role of NAA in myelination. The nur7 transgenic mouse (Traka et al., 2008) selected for the current study recapitulates the essential clinical features of Canavan disease without extraneous pathology not reported in the human disease (Ahmed et al., 2016). The ability to target oligodendrocytes in nur7 mice would contribute greatly to both our understanding of the role of NAA in myelination and the definition of endpoint measures of clinical relevance. We present here the application of a next-generation "oligotropic" AAV vector to the nur7 model and show profound improvements in white matter integrity and motor function are associated with the correction of early energetic deficit following the reconstitution of ASPA in oligodendrocytes. The clinical significance of early metabolic rescue in this pre-clinical model is supported by correlative data from human siblings harboring an R71H *Aspa* mutation associated with unusually mild Canavan disease (Janson et al., 2006a), suggesting an underlying compromise in oxidative white matter respiration is of direct relevance to phenotype. These results support a model in which loss of bioavailable NAA leads to defining early energetic stress, which is reversible through normalization of NAA metabolism in the oligodendroglial compartment specifically.

2. Results

2.1. Targeted transduction of oligodendroglia in vivo with "oligotropic" AAV-Olig001

A novel oligotropic AAV gene delivery system (AAV-Olig001) was generated by a directed evolution screening process to identify viable variations in vector capsid promoting oligodedroglial tropism. After in vitro validation (data not shown), in vivo oligodendroglial tropism was quantified. An AAV-Olig001-GFP reporter vector was injected into the corpus callosum of adult wild type mice and tropism scored by dual-label immunofluorescence (Fig. 1A). Approximately 90% of GFP-positive cells in the brains of transduced animals co-labeled with the oligodendrocyte-specific antigen Olig2, 7% positive for NeuN, and 3% positive for GFAP, thus confirming the tropism of AAV-Olig001 for white matter-producing cells (Fig. 1B). AAV-Olig001-GFP was then administered to postnatal day 2–3 (P2–3) animals via intraparenchymal injection to target precursor and immature oligodendrocytes in subcortical white matter tracts (Sauvageot and Stiles, 2002). Widespread GFP fluorescence was observed two-weeks post-transduction, with strong GFP labeling of white matter tracts (Fig. 1C) and outlying gray matter-rich areas of transduced brains which co-labeled with Olig2 (Fig. 1D).

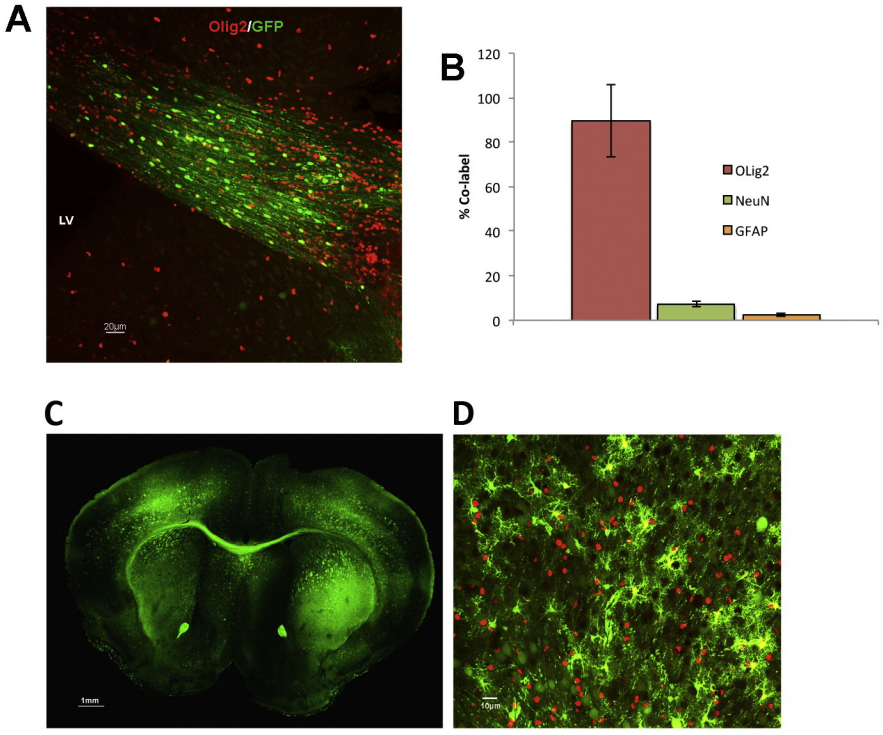

Fig. 1. Oligodendroglial tropism of AAV-Olig001. (A) Native GFP fluorescence in the corpus callosum of an animal transduced with AAV-Olig001-GFP (B) Serial sections of AAV-Olig001-GFP-transduced brains were scored for co-labeling with oligodendrocyte (Olig2), neuronal (NeuN), or astrocytic (GFAP) antigens to assess tropism. Mean percentage of GFP-positive cells co-labeling with each antigen presented ($n = 3$, mean ± sem). Over 90% of GFP-positive cells co-label with Olig2. (C) Global transduction of neonatal brains with AAV-Olig001-GFP. Native fluorescence shown in a brain 2-weeks post transduction highlighting strong labeling of subcortical white matter tracts, motor cortex, and basal ganglia. (D) GFP-positive cells within the motor cortex have oligodendroglial morphology and co-label with Olig2 (red).

2.2. Restoration of early energetic deficit

Gross neuropathology and oligodendrocyte loss in nur7 mice is first evident at 3 weeks of age (Traka et al., 2008) and is preceded by energetic stress (Francis et al., 2012). A codon-optimized human *ASPA* cDNA was packaged into the AAV-Olig001 system for delivery to nur7 mice at postnatal day 2–3 (P2–3). Vector was administered via the intraparenchymal route, using methodology identical to that employed for tropism studies (Fig. 1C&D). AAV-Olig001-ASPA transduced brains were analyzed by HPLC for whole-brain NAA content at 2 weeks of age to confirm ASPA transgene functionality. AAV-Olig001-ASPA brains had a significant two-fold reduction in NAA relative to both AAV-Olig001-GFP nur7 and naïve nur7 negative controls (ASPA = 5.095 ± 0.24 mMol/g; GFP = 8.65 ± 0.28 mMol/g, naïve = 8.8 ± 1.08 mMol/g), clearly visible on chromatograms (Fig. 2B & C) bringing whole brain NAA to within the range of wild type (4.22 ± 0.42 mMol/g) references (Fig. 2A). Concurrent with reduced NAA was a significant increase in both acetyl coenzyme A (AcCoA; Fig. 2D), reflecting increases in bioavailable acetyl groups, and malonyl coenzyme A (MalCoA; Fig. 2E), the committed step of entry of AcCoA to fatty acid synthesis. Because fatty acid synthesis and the Krebs cycle share a substrate requirement for AcCoA, we hypothesized that the provision of ASPA to developing nur7 oligodendrocytes would act to uncouple myelination from energetic metabolism. AMP, ATP, and reduced and oxidized glutathione (GSH, GSSG) were analyzed by HPLC in 2 week old AAV-Olig001-ASPA transduced brains. We observed a two-fold increase in ATP content in AAV-Olig001-ASPA brains (Fig. 2F) (wild type ATP = 4.15 ± 0.521 μMol/g; nur7 GFP = 2.05 ± 0.199 μMol/g; nur7 ASPA = 3.31 ± 0.397 μMol/g) and an ATP/AMP ratio that was not significantly different from wild type controls (Fig. 2G), indicating the rescue of early energetic abnormalities. In addition, a significant increase in the ratio of reduced to oxidized glutathione (GSH:GSSG) in AAV-Olig001-ASPA brains (Fig. 2H) suggested this improved energetic status resulted in a reduction in oxidative stress.

2.3. Oligodendroglial ASPA reconstitution rescues motor deficit

In order to ascribe phenotypic significance to the observed rescue of early energetic improvements, AAV-Olig001-ASPA transduced animals were tested on an accelerating rotarod for latency to fall at 12 weeks of age and compared with negative and age-matched wild type reference animals (Fig. 3A). ASPA-transduced animals demonstrated an improvement in rotarod performance (nur7 ASPA = 274 ± 13.2 s; nur7 GFP = 152 ± 8.0 s; $p = 0.0015$) that was not significantly different from wild type (295 ± 11.37 s). At the conclusion of rotarod testing, animals were assessed for daily activity patterns over a week using automated activity wheels. AAV-Olig001-ASPA-transduced animals demonstrated a highly significant ($p = 0.00021$) improvement in daily activity (Fig. 3B & C). Both AAV-Olig001-ASPA and AAV-Olig001-GFP animals had normal 24-h daily cycles with identical nocturnal active periods, indicating that differences in activity were not due to differences in circadian rhythms. Rotarod and activity data indicate the

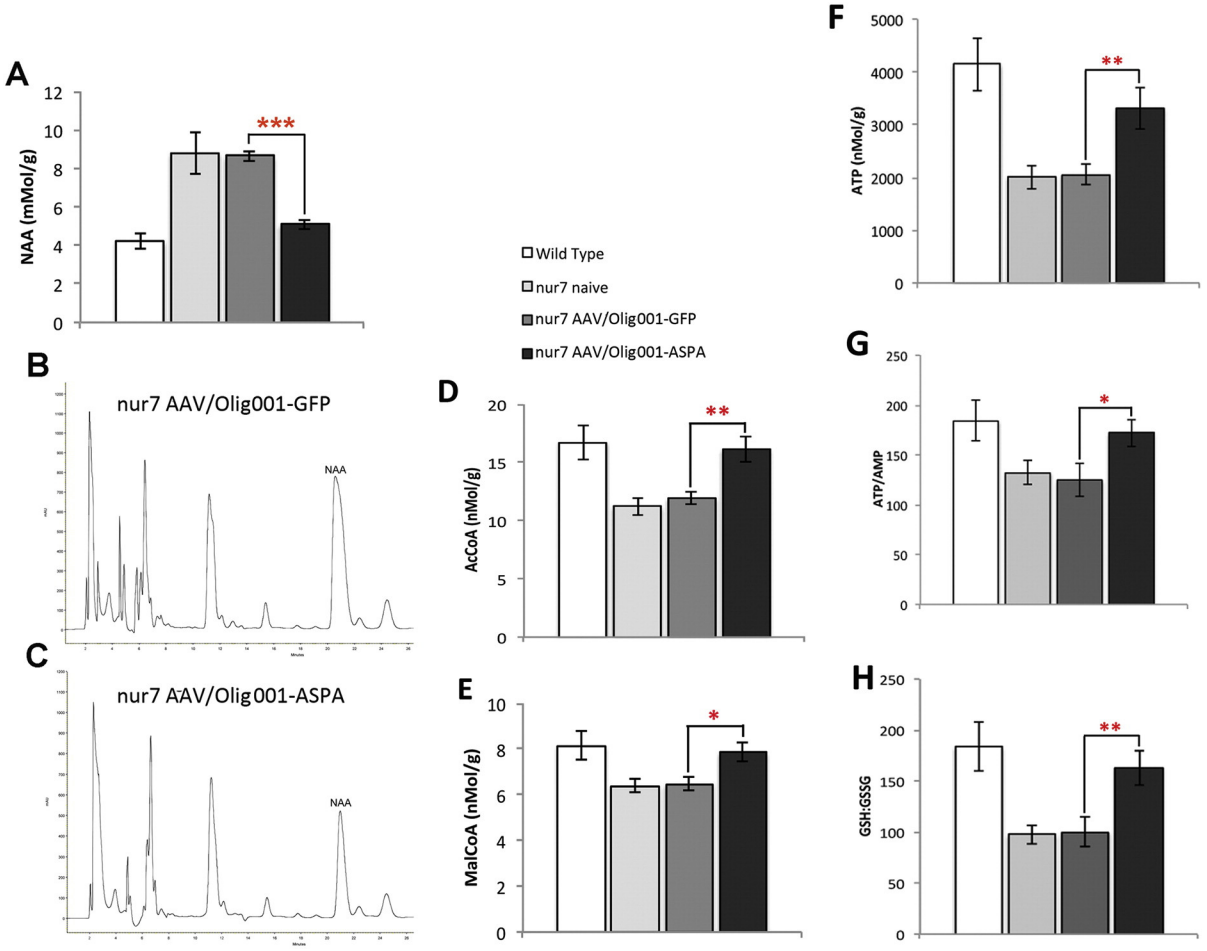

Fig. 2. Rescue of metabolic defects in the nur7 brain. (A) Reductions in whole brain NAA in 2-week old AAV-Olig001-ASPA brains to near age-matched wild type levels (***$p < 0.001/n = 5$). Representative chromatograms of AAV-Olig001-GFP (B) and AAV-Olig001-ASPA brains (C). Rescue of whole brain AcCoA (D) MalCoA (E) levels in the same brains with simultaneous recovery of ATP (F), ATP/AMP ratios (G) and GSH:GSSG ratio (H). *$p < 0.01$, mean ± sem shown. Significance between groups determined using Two-tails Student's *t*-test.

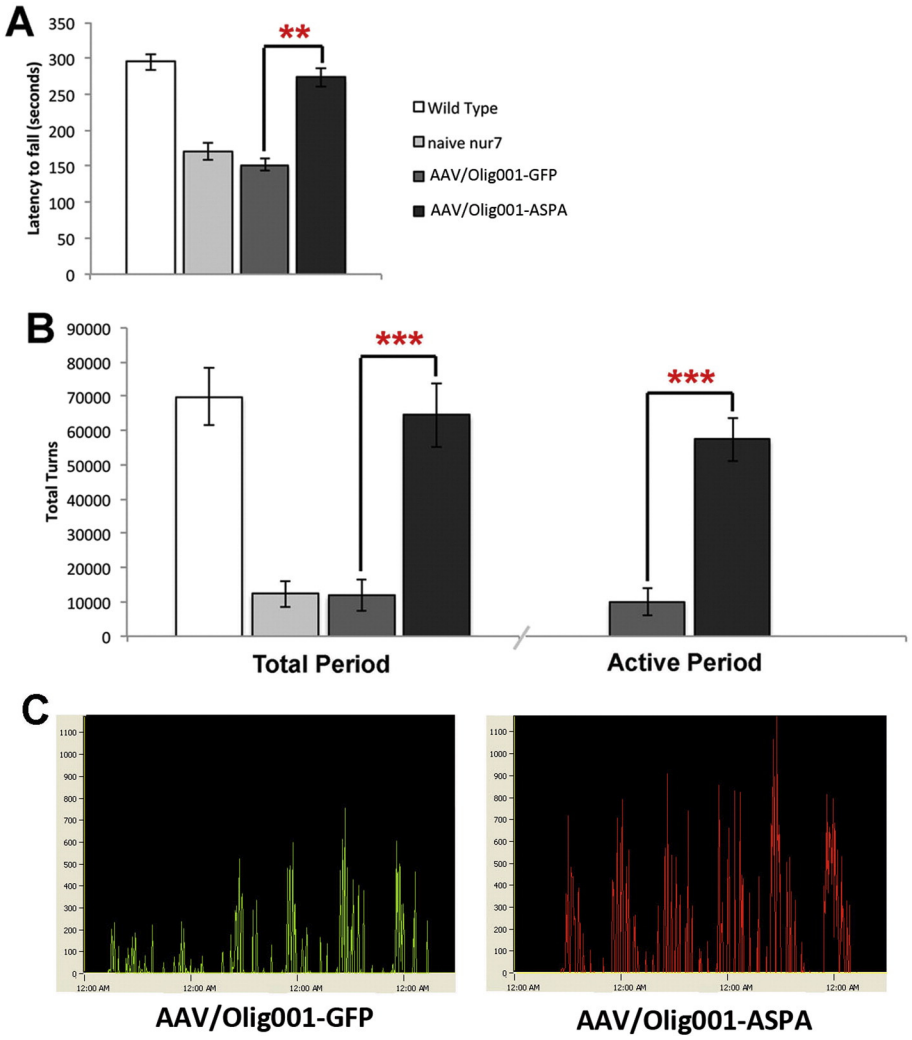

Fig. 3. Rescue of motor function by AAV/Olig001-ASPA. (A) AAV/Olig001-ASPA animals presented with a highly significant increase in latency to fall on an accelerating rotarod at 12 weeks of age ($n = 10$/treatment group; $^{**}p < 0.01$). (B) At the conclusion of rotarod testing, the same animals were assessed for daily activity patterns over a 7 day period using automated running wheels. Activity, measured in wheel turns, was vastly increased in AAV/Olig001-ASPA animals both over the entire 7 day period and during the active nocturnal period of the daily cycle ($^{***}P < 0.001$; n = 10). (C) Representative actograms for AAV/Olig001-GFP (green) and AAV/Olig001-ASPA (red). Mean ± SEM presented with significant differences between groups determined by Two-tailed Student t-test.

complete rescue of motor deficit by AAV-Olig001-ASPA is associated with early metabolic rescue.

2.4. AAV-Olig001-ASPA promotes normal myelination and corrects vacuolation

At the conclusion of activity testing, animals were sacrificed and brains processed for myelin basic protein (MBP) staining to provide an index of myelination in treated and control brains. This revealed a dramatic brain-wide increase in myelin content in AAV-Olig001-ASPA brains indistinguishable from wild type controls (Fig. 4A-F). As the rotarod test is a sensitive measure of cortical integrity (Hamm et al., 1994), including that determined by MBP content (Kuhn et al., 1995), we quantified MBP length density (MBP-LD) in the motor cortex of treated and control brains by unbiased stereology. Estimates of MBP LD revealed an increase in AAV-Olig001-ASPA brains relative to controls that was again indistinguishable from wild-type (wild type = 0.057 ± 0.0056 μm/mm^3; ASPA nur7 = 0.053 ± 0.0046 μm/mm^3; GFP nur7 = 0.031 ± 0.0038 μm/mm^3) (Fig. 4G & H). Areas of treated brains that characteristically present with intense vacuolation manifest a striking increase in MBP (Fig. 4B). Serial H&E stained sections processed in AAV-Olig001-ASPA brains to quantify thalamic vacuole area fraction by unbiased stereology (Fig. 5G), revealed complete rescue of vacuolation. Both naïve and AAV-Olig001-GFP nur7 brains had a near 20% loss of thalamic volume to vacuolation (17.25$^{\pm}$2.2% and 16.82 ± 1.7%, respectively) (Fig. 5A&G), which correlated with abnormal MBP staining (Fig. 5B, D, F). AAV-Olig001-ASPA nur7 brains exhibited 0.08% vacuolation of the thalamus (Fig. 5C&D), which was not significantly different from wild type reference controls (0.10%), and can likely be attributed to artifact from immunohistochemical processing.

White matter in the brain is produced by oligodendroglia. Given the increase in MBP density in nur7 AAV-Olig001-ASPA brains (Fig. 4), it is likely that the reconstitution of ASPA activity in nur7 mice promotes oligodendroglial viability. Consistent with this, areas of the nur7 brain that manifest vacuolation, such as the medial septum (Fig. 6A) and the thalamus (Fig. 6B), showed increases in staining for the late-stage oligodendrocyte marker CC1. The medial septum and thalamus of AAV-Olig001-ASPA brains were sampled using unbiased stereology for CC1-positive cell numbers, which revealed a significant 2-fold increase in the medial septum (Fig. 6C) three-fold increase in the thalamus (Fig. 6D). Numbers of thalamic APC-positive cells in AAV-Olig001-ASPA brains (97,856.53 ± 12,937) were nearly 90% of age-matched wild

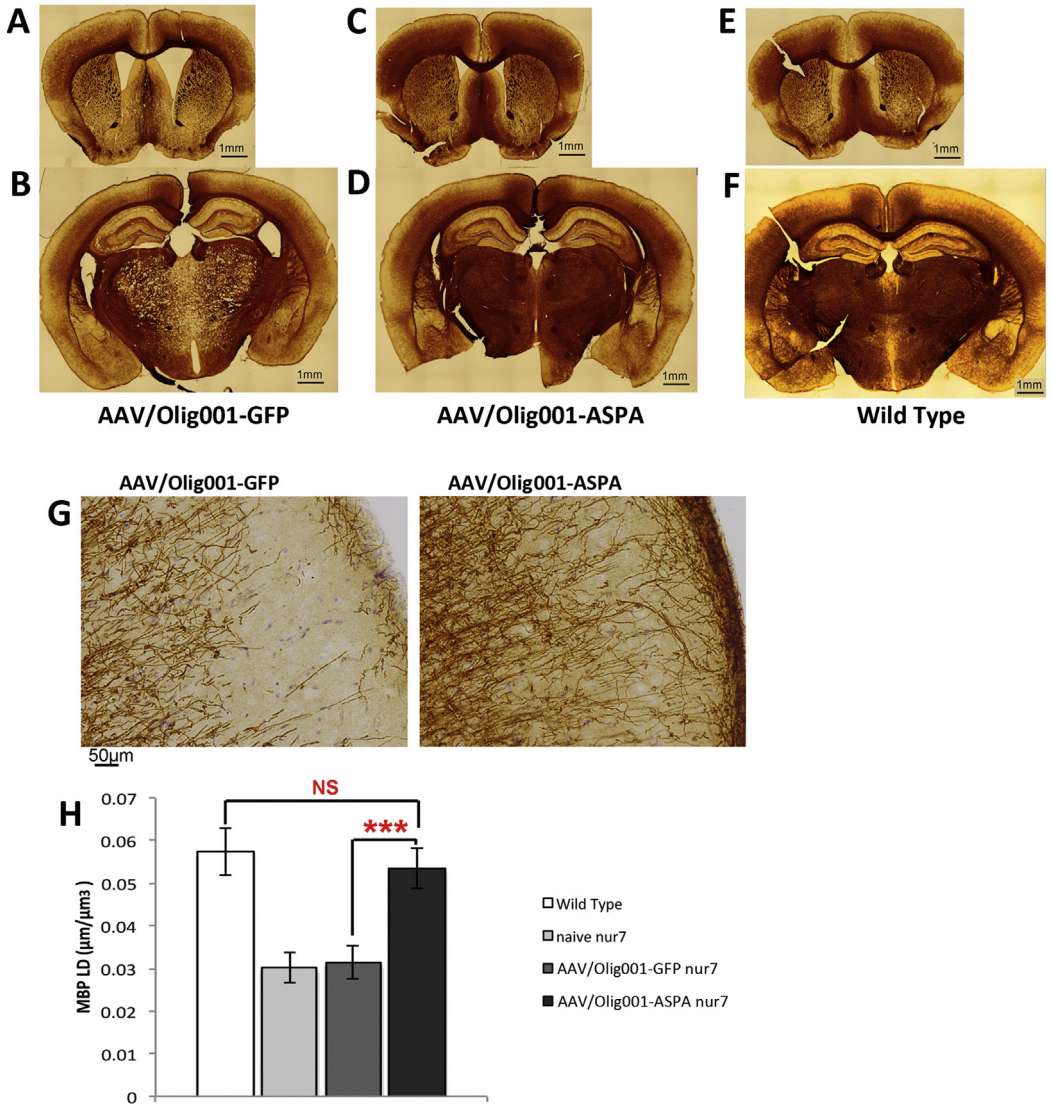

Fig. 4. Rescue of myelination by AAV/Olig001-ASPA. MBP staining in 12-week old AAV/Olig001-ASPA brains (C&D) revealed a drastic improvement in MBP density relative to controls (A&B). Improvements in MBP density were especially noticeable in areas of the brain such as the thalamus (B&D) that are associated with intense vacuolation. MBP staining in AAV/Olig001-ASPA brains was indistinguishable from age-matched wild type reference brains (E&F). MBP fiber length density (MBP-LD) in the motor cortex of AAV/Olig001-ASPA brains was significantly higher than controls (G), and quantification by stereology (H) revealed cortical MBP-LD rescue to wild type levels. MBP-LD expressed in $\mu m/mm^3$ (volume of area sampled) with the mean ± SEM for 5 animals per treatment group shown. ***$p < 0.001$, NS = not significant. Significance between groups determined by Two-tailed Student's t-test.

type levels as compared to AAV-Olig001-GFP brains (36,554.12 ± 4514.4), which were only 37% of wild type numbers (110,251 ± 8699). Using DAPI counterstain to label cell nuclei, the same sections were scored for total cell numbers (Fig. 6E). Total (DAPI-positive) cell numbers in the AAV-Olig001-ASPA nur7 thalamus were not significantly different from wild type reference controls (94%), while AAV-Olig001-GFP total thalamic numbers were only 50% of wild type, suggesting that the cell loss in the nur7 thalamus primarily affects the oligodendroglial lineage. Finally, 12-week brains were immunostained for ASPA and processed for HPLC to confirm the longer-term expression and functionality of AAV-Olig001 delivered ASPA. Robust ASPA staining was seen in both subcortical white matter tracts (Fig. 7A) and outlying gray matter-rich areas (Fig. 7C) of AAV-Olig001-ASPA transduced brains. There was a complete absence of ASPA staining in all areas of control nur7 brains (Fig. 7B, D). ASPA staining in AAV-Olig001-ASPA brains also co-localized with Olig2 in 12-week old animals (Fig. 7 E, F, G), thereby confirming persistent expression in oligodendrocytes. Whole brain NAA levels in AAV-Olig001-ASPA animals were significantly lower than controls, and not indistinguishable from age-matched wild type references, (Fig. 7H) indicating long term metabolic correction.

2.5. Human correlative data suggests metabolic stress in typical Canavan disease, with a benign pattern in mild Canavan disease

AAV-Olig001-ASPA intervention in the nur7 mouse resulted in increased acetyl-CoA and improvements in ATP/AMP ratio, in conjunction with decreases in global NAA, which suggests a shift toward aerobic respiration. Previously, we had described two sisters with an unusually mild presentation of Canavan disease, due to compound heterozygosity with R71H mutation (Janson et al., 2006a). Both sisters have been followed since diagnosis and remain developmentally appropriate for age. As part of ongoing surveillance we tested brain lactate levels using multi-voxel imaging, while simultaneously measuring NAA using precise single-voxel imaging. We found significant differences (Fig. 8) between NAA/creatine ratios of both mildly affected sisters

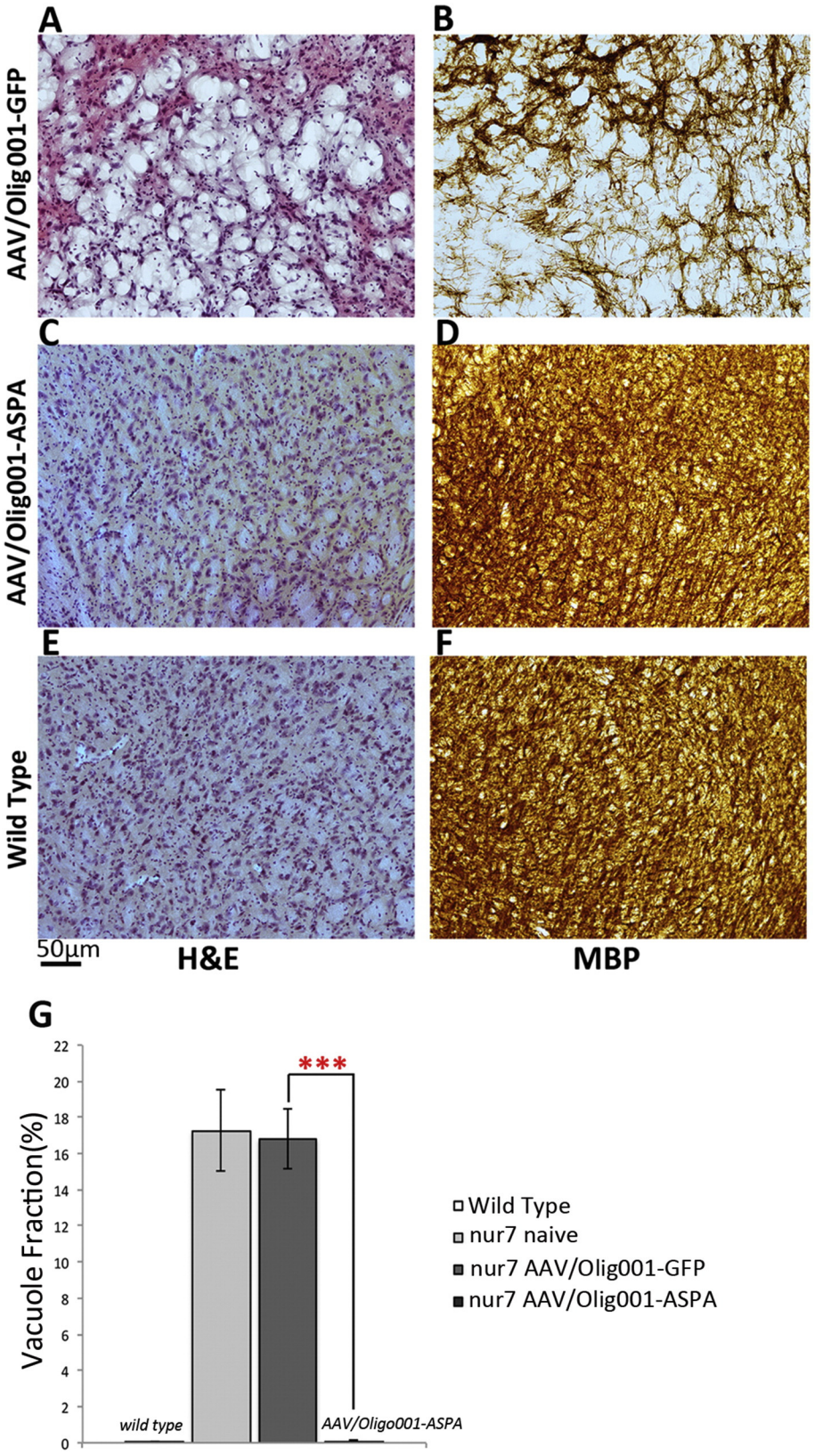

Fig. 5. Rescue of vacuolation by AAV/Olig001-ASPA. Brains of 12-week old animals were serially processed for H&E staining. The thalamus of AAV/Olig001-ASPA brains (C) is indistinguishable from wild type reference brains (E), and contrasts drastically with the intensely vacuolated AAV/Olig01-GFP thalamus (A). Thalamic H&E staining closely mirrors MBP staining (B, D, F). (G) Stereological estimates of thalamus vacuole volume fraction reveal a complete rescue in AAV/Olig001-ASPA nur7 brains, with no significant difference to age-matched wild type reference controls. $^{***}p < 0.001$, n = 5/group. Significant differences between group means (±SEM) determined using Two-tailed Student's t-test.

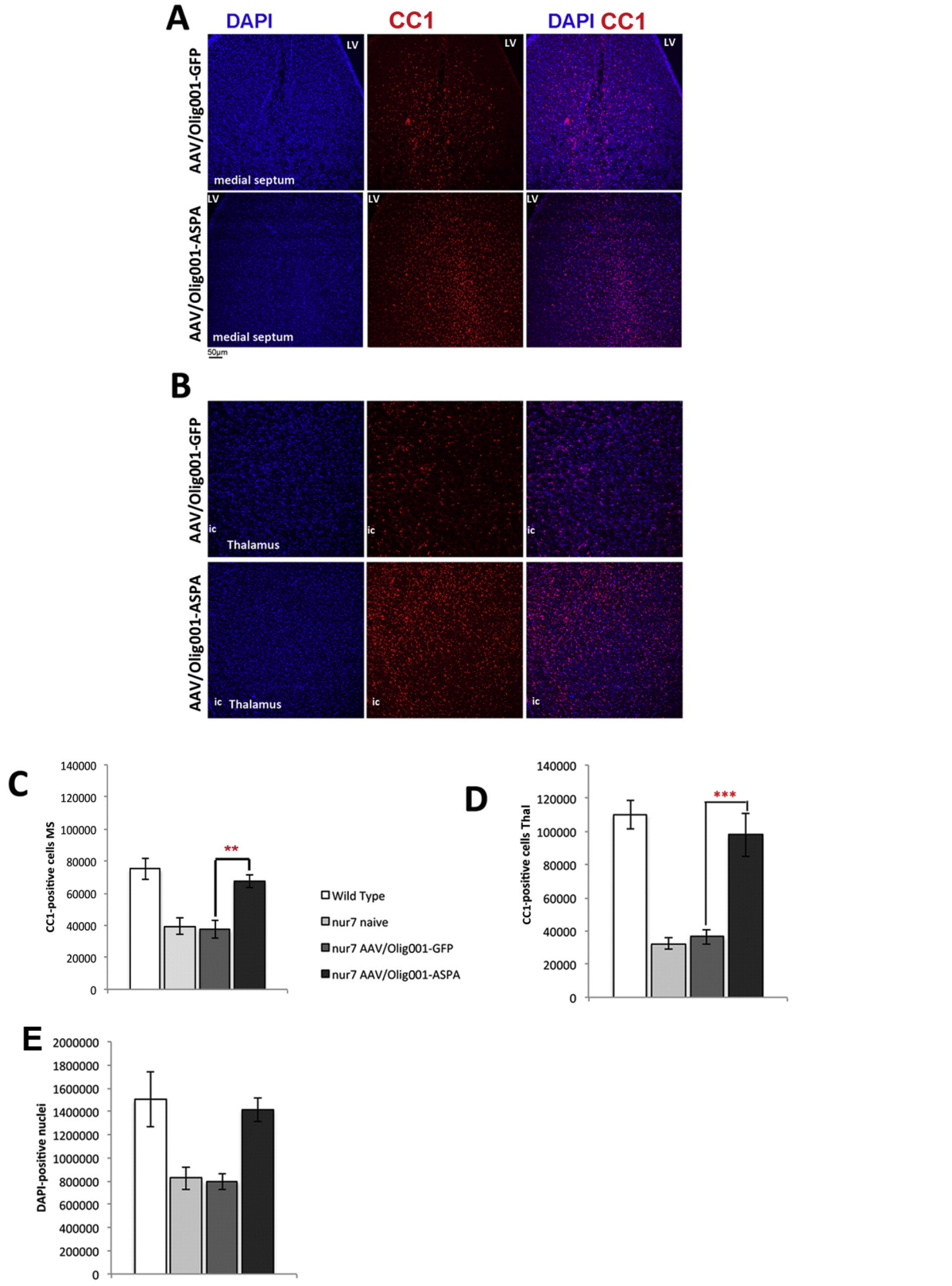

Fig. 6. Rescue of vacuolation in AAV/Olig001-ASPA nur7 brains is associated with increased oligodendrocyte content. Fluorescent immunolabeling of total nuclei (DAPI) and late stage oligodendrocytes (CC1) in the medial septum (A) and thalamus (B) showing significant increases in CC1-positive cells in AAV/Olig001-ASPA nur7 brains relative to GFP controls. Stereological estimates of CC1 cell numbers in both the medial septum (MS) (C) and thalamus (Thal) (D) revealed the restoration of CC1 content to near wild type levels in AAV/Olig001-ASPA brains. Counts of thalamic DAPI-positive nuclei (E) on the same sections indicate deficiencies in cell number are mainly accounted for by absent oligodendrocytes. ***$p < 0.001$, **$p < 0.01$, $n = 5$/group, mean ± SEM shown. Significant differences between groups determined by Two-tailed Student's t-test.

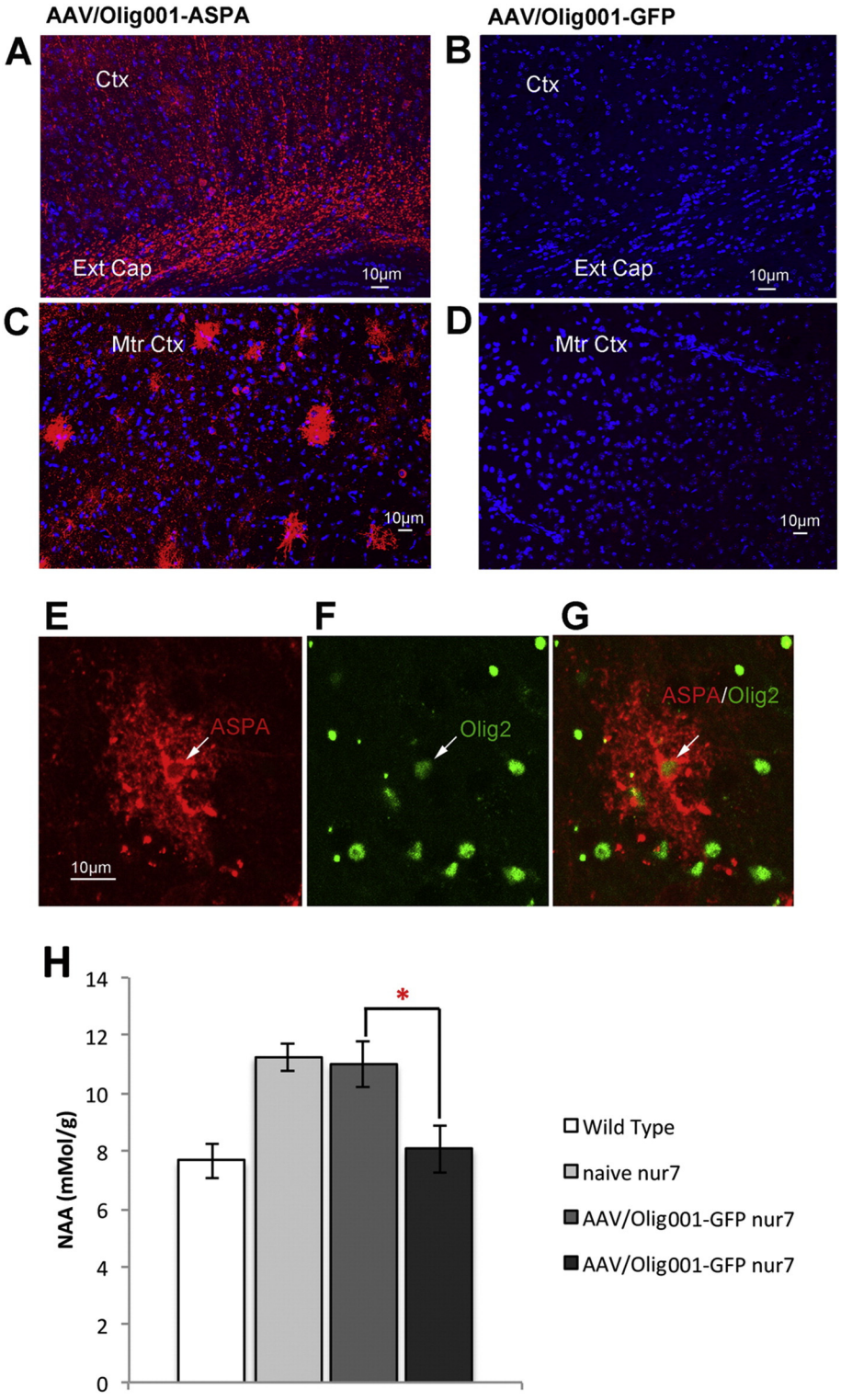

Fig. 7. Long term ASPA transgene expression in the nur7 brain. 12-week old brains from AAV/Olig001-ASPA (A&C) and AAV/Olig001-GFP (B&D) nur7 brains stained for ASPA (red) and counterstained with DAPI (blue). White matter tracts of the external capsule (Ext Cap) of AAV/Olig001-ASPA brains (A) labeled stringly for ASPA-positive fibers, with no detectable staining in white matter tracts of AAV/Olig001-GFP nur7 brains (B). Outer layers of the motor cortex (Mtr Ctx) of AAV/Olig001-ASPA nur7 brains also contained densely stained, multi process-bearing ASPA-positive cells (C), with a total absence of cortical ASPA staining in AAV/Olig001-GFP nur7 brains (D). Individual ASPA-positive cells in AAV/Olig001-ASPA brains (E) co-labeled with Olig2 (F&G) indicating persistent oligodendrocytic transgene expression. (H) HPLC performed on 12-week old brains confirmed long term transgene functionality, with a significant reduction in whole brain NAA shown in AAV/Olig001-ASPA nur7 brains relative to controls. $^{*}p < 0.05$, $n = 4$/group.

compared to severely affected Canavan patients (age 15–24 months), as well as significant differences in the lactate content of white matter. Genomic DNA isolated from whole blood samples from both R71H patients confirmed the absence of mutations in *Nat8L* (data not shown), controlling for genetic abnormalities that may confound the interpretation of NAA levels. Also of note, we found that until the age of six months, lactate levels (as measured with CSI) are quite similar in mild and typical Canavan disease, at which point lactate levels in

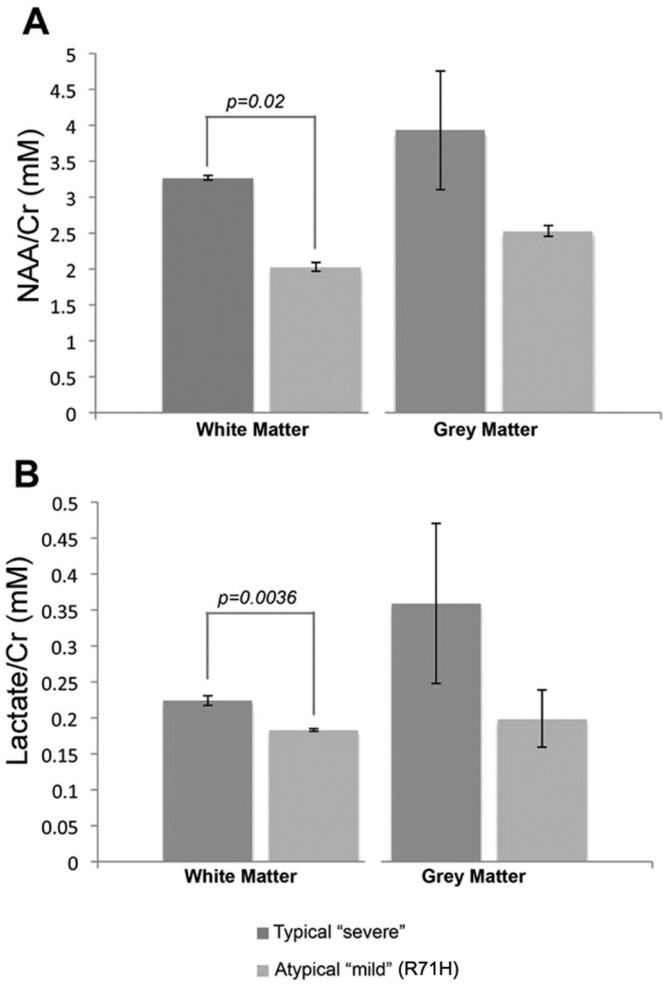

Fig. 8. Chemical shift imaging of NAA and lactate in brains of severely affected (n = 3, age 15–24 months) and atypically mild ($n = 2$, ages 5 and 8 years) Canavan patients. Severely affected patients carried heterozygous compound mutations in the ASPA gene; mild patients were compound heterozygotes for the R71H mutation. The same patients were imaged using both single voxel 1H–MRS for NAA and chemical shift imaging (CSI) for lactate quantification, as per established protocols. There is a significant difference in mean values for lactate in white matter between mild and severely affected patients ($p < 0.05$, Student's two-sample t-test with 3df) with increasing whole brain NAA, suggesting that more severe Canavan disease favors anaerobic respiration in white matter and may be associated with metabolic stress.

homozygous Canavan patients significantly increases (data not shown). This trend parallels NAA increases in typically severe cases but not in the R71H siblings, suggesting progressive metabolic dysregulation is defined by increases in lactate at least as much as it is by NAA.

3. Discussion

Unlike neuronal transgene expression seen with previous studies (Ahmed et al., 2013) (Klugmann et al., 2005) (McPhee et al., 2005) (Matalon et al., 2003), the present study successfully reconstituted ASPA in its natural compartment. Evidence of abnormalities in oxidative metabolism upstream of gross pathology associated with chronically elevated NAA in Canavan disease (Francis et al., 2012) invite a comparison with a significant body of published data suggesting low NAA equates to impaired energetic integrity (Moffett et al., 2007). Oligodendrocytes are vulnerable to low energy conditions that impair function (Rinholm et al., 2011), and the present study suggests compromised oligodendrocyte integrity in the setting of Canavan disease is of relevance to the role of NAA in myelination. Oligodendrocytes engage in a significant degree of metabolic reciprocity with neurons to maintain homeostasis under conditions of energy deprivation (Funfschilling et al., 2012). The rescue of AcCoA, MalCoA, and ATP by AAV-Olig001-ASPA in nur7 mice provides evidence for NAA catabolism contributing to both myelination and oxidative metabolism, and suggests NAA acts as an energy shuttle from the axon to the oligodendrocyte, thereby building on a theme of neuro-glia metabolic coupling. Glycolytic AcCoA contributes to myelin lipid synthesis, with a portion of this requisite substrate provided to oligodendroglia in the form of NAA (D'Adamo and D'Adamo, 1968) (Burri et al., 1991). In the absence of NAA, the resultant diversion of glucose-derived AcCoA to fatty acid synthesis is hypothesized to result in a net loss of ATP (Harris and Attwell, 2012). ASPA is required for NAA to contribute substrate for fatty acid synthesis, which predicts adverse energetic consequences for the loss of ASPA function in Canavan disease. The rescue of oxidative metabolic abnormalities in nur7 mice by AAV-Olig001-ASPA is consistent with this hypothesized net energetic loss, lending support to the use of non-invasive markers of cerebral glucose metabolism in future clinical trials for Canavan disease.

Relatively more modest improvements reported for other gene therapy interventions bear closer scrutiny (Ahmed et al., 2016) (Klugmann et al., 2005). The lack of evidence of direct benefit to oligodendrocytes in these interventions is likely attributable to tropism and cell-specific effects obtained with AAV-Olig001. While improvement has been reported with systemic intravenous delivery using neurotropic AAV, those studies (Ahmed et al., 2013), unlike the present, did not use unbiased stereology to quantify the association between improvements in histopathology and vector tropism, making it difficult to assess direct effects on end points of direct relevance to myelination. A reliance on the assumption that NAA is the primary index of pathology in Canavan disease results in an emphasis on atypical findings (Ahmed et al., 2016), which are not manifest in the clinical population (McPhee et al., 2006). While the enigmatic nature of NAA function currently accommodates these speculative mechanisms, we would argue end points generated by the physiologically appropriate reconstitution of ASPA using AAV-Olig001 in the present study offer a more direct and reproducible index of NAA function during developmental myelination. In this context, it should be noted that the present study did not directly assess histopathology in non-targeted areas of the brain, such as the cerebellum and brain stem that characteristically present with vacuolation, and there is some scope for improvement of the definition of end point measures that are relevant to phenotypic rescue of a model system that presents with global abnormalities in the CNS. However, the clear improvements in metabolic indices taken from whole treated brains suggest oligodendroglial targeting is a significant improvement on previous neurotropic vectors. Future studies will likely require an assessment of the relationship of vector spread to the integrity of specific anatomical compartments in older animals that are post developmental myelination.

The acetate moiety of NAA incorporated into myelin lipids (Burri et al., 1991) via ASPA (Chakraborty et al., 2001) is not rate limiting for myelination, as myelin is produced in Canavan disease patients and ASPA null rodent models. Moreover, a case study of a child without detectable NAA showed only moderately delayed myelination (Martin et al., 2001). The abovementioned child exhibited a loss of function mutation in NAA synthase (*Nat8L*; (Wiame et al., 2010), suggesting NAA is not an absolute requisite, raising the possibility of elevated NAA being directly toxic to white matter.

To determine if myelination in the setting of Canavan disease could be improved by targeting NAA synthesis independently of ASPA, Guo et al. (2015) generated nur7/*Nat8L*–null double mutants that produced neither NAA nor ASPA and presented improvements in myelination and motor function, suggesting that loss of *Aspa* was secondary to pathological levels of accumulated NAA. Maier et al. (2015) likewise reported ostensibly similar double mutants that presented with extended lifespan. The original presentation of the nur7 mouse model documents consistent survival up to at least 20 weeks of age (Traka et al., 2008). Our own experience with this model (Francis et al., 2012) (Francis et al.,

2014), including the present study, does not support claims of premature death of the nur7 mouse at 4 weeks of age. In addition, mice null for the aralar1 subunit of the malate-aspartate shuttle present with abnormally low NAA and hypomyelination as a consequence of reduced substrate for NAA synthesis (Ramos et.al. 2011), conflicting claims of normal myelination in *Nat8L* null mutants. These inconsistencies do not preclude consideration of direct effects resulting from elevated NAA, but given the association of abnormally low NAA with pathology in numerous non-Canavan disease contexts, the ablation of Nat8L activity in neurons is arguably non-specific. A possible compromise to be made in this context is the fact that NAA synthesis relies on mitochondrial aspartate that also fuels the transfer of cytosolic reducing equivalents to mitochondria for oxidative phosphorylation (McKenna et al., 2006). The ablation of *Nat8L* may therefore result in a net energy saving by preserving metabolic substrate in a manner similar to our hypothesized role for ASPA-derived acetyl groups during myelination (Francis et al., 2012). Indeed, NAA synthesis is already downregulated in Canavan disease (Moreno et al., 2001), which potentially compensates for the compromised contribution of NAA to the energetic demands of myelination (Harris and Attwell, 2012). The claims of the present study and those of Guo et al. (2015)) and Maier et al. (2015) may therefore find common ground in a focus on overall energetic integrity. Using the quantitative metabolic, histopathological, and behavioral endpoints presented here, future studies will be able to assess the relative effects of acetate deprivation and NAA toxicity more directly to provide a more nuanced view of NAA function of general relevance to metabolic integrity in the central nervous system.

4. Materials and methods

4.1. Cloning of functional ASPA and packaging into oligotropic AAV

A codon optimized human *ASPA* cDNA was designed and synthesized using a commercially available algorithm tool (Integrated DNA Technologies, Coralville, IA, USA) and subcloned into plasmid pTRS-KS-CBh-GFP (National Gene Vector Biorepository), to generate pTRS-KS-CBh-ASPA. AAV-Olig001 capsid used to package pTRS-KS-CBh-ASPA was developed in the laboratories of S. Gray and T. McCown at the University of North Carolina at Chapel Hill, through a directed evolution screening process similar to that described (Gray et al., 2010). AAV-Olig001 vector used in these studies packaged a self-complementary (sc) genome with transgene expression mediated by the CBh promoter and bovine growth hormone polyA (Gray et al., 2011). AAV vectors were produced using methods developed by the University of North Carolina Vector Core facility, as previously described (Clement and Grieger, 2016). In brief, production plasmids (pXX6–80, pTRS-KS-CBh-EGFP or pTRS-KS-CBh-ASPA, and pXR-Olig001) were triple-transfected into suspension HEK293 cells. AAV vectors were purified from cells by iodixanol gradient centrifugation, followed by ion-exchange chromatography. AAV was dialyzed in PBS supplemented with 5% D-Sorbitol and an additional 212 mM NaCl (350 mM NaCl total). Genomic titer was determined by quantitative PCR and confirmed by PAGE and silver stain.

4.2. Animals

Nur7 mice were obtained commercially (Jackson Laboratory, Bar Harbor, ME, USA), and maintained at Rowan SOM animal facility under IACUC approval. All studies were conducted in accordance with the United States Public Health Service's Policy on Humane Care and Use of Laboratory Animals. Homozygous nur7 animals were generated by pairing of heterozygotes and genotyped using a custom SNP real time qPCR assay. AAV vectors were administered to isoflurane-anesthetized adult animals using stereotactic coordinates. A sterile 10 μl Hamilton syringe was introduced to the corpus callosum and 0.5 μl (2×10^{12} viral genomes/ml) of AAV-Olig001 was delivered at a rate of 0.1 μl/min using a digital infusion pump. Neonatal surgeries were performed on P2–3 cryoanesthetized animals. Animals were placed in a custom epoxy body mold and a sterile 5 μl Hamilton syringe was directed to coordinates targeting the cingulum (−1.2 mm DV) and internal capsule (−2.4 mm DV) of both cerebral hemispheres (i.e., 4 injections per animal). Each injection consisted of 0.5 μl of a 2×10^{12} vg/ml vector stock, which yields 4×10^{9} vg per animal. Injections were performed with a digital infusion pump at a rate of 0.25 μl/min.

4.3. Clinical subjects

All data were obtained under IRB-approved research protocols. Patients underwent MRI and proton spectroscopy (H_1-MRS) at Children's Hospital of Philadelphia. H_1-MRS provides a non-invasive method of performing quantitative and semi-quantitative measurements of brain metabolites. There are two techniques commonly used to detect NAA and other metabolites, multi-voxel chemical shift imaging (CSI) and single-voxel spectroscopy (SVS). Our group has used SVS extensively in the past, which provides a greater level of sensitivity but is unable to quantify lactate due to contamination by lipid signals. For this comparison, subjects were imaged twice on a Siemens 1.5 T magnet at Children's Hospital of Philadelphia using SVS with STEAM pulse sequence to detect NAA and using CSI to detect lactate. Two mildly affected patients with R71H mutation were compared to three severely affected patients with common mutations, and mean metabolite levels were compared using Student's *t*-test. Sequencing of *Nat8L* was performed on genomic DNA isolated from whole blood taken from both mildly affected patients under approved IRB guidelines. Raw sequence data was generated using a commercial facility (Genewiz, South Plainfield, NJ) and homology with the deposited normal CDS confirmed with Vector NTI® software (ThermoFisher Scientific, Waltham, MA).

4.4. HPLC

All target metabolites in mouse brains were analyzed in a single run as previously described (Lazzarino et al., 2003), and sample sizes for all HPLC end points are identical. Samples were prepared from tissue flash frozen in liquid nitrogen. Frozen brains were homogenized in an acetonitrile K_2HPO_4 (10 mM) precipitation solution (3:1 v/w), extracted twice with chloroform, and stored at −80 °C until analyzed. 50 μL of each sample was run on a Thermo Scientific HPLC system equipped with a Surveyor PDA plus UV detector, a Hypersil BDS-C18 column (5 μm particle size; 25 cm × 4.9 mm), and analyzed with ChromQuest software (Thermo Scientific). Target metabolites in samples were quantified against reference standards. Data is presented as the mean per group ± the standard error of the mean in all HPLC graphs.

4.5. Immunohistochemistry

Immunohistochemistry was performed on 40 μm free-floating sections. Animals were anesthetized and transcardially perfused with ice-cold 0.9% saline followed by 4% buffered paraformaldehyde (PFA). Perfused brains were removed and post fixed in 4% PFA overnight, then cryoprotected in an ascending sucrose gradient. Cryoprotected brains were flash frozen and stored at −80 °C until processed. The entire forebrain was serially sectioned and maintained in sequence for subsequent stereological sampling. Immunohistochemistry for CC1, Olig2, GFAP, NeuN, and MBP was performed using commercially available antibodies (EMD Millipore, Gibbstown, NJ, USA). ASPA antibody was custom-made as previously described (Francis et al., 2011). GFP co-labeling with Olig2, NeuN, and GFAP for tropism analysis employed laser-scanning confocal microscopy and scoring co-labeled GFP-positive cells in *Z*-stacks. Three individual brains transduced with GFP reporter vector were serially sectioned 1 mm anterior and 1 mm posterior from bregma (~25 sections total). Every third section was stained for either Olig2, NeuN, or GFAP and processed using CY3-conjugated secondary antibodies (EMD

Millipore Gibbstown, NJ, USA). A region of interest (ROI) measuring 1 mm × 1 mm was delineated within the corpus callosum of each section in each series and Z-stacks were generated every 500 μm^2 within the ROI (10 μm depth, step size of 2 μm). Total numbers of GFP-positive cells were scored within Z-stacks using Nikon NIS elements software and GFP-Olig2/NeuN/GFAP co-labeled cells were expressed as a percentage of GFP-positive.

4.6. Stereology

Estimates of N for APC and DAPI in sections were performed using the optical fractionator (k = 4). APC was visualized using a Cy3-conjugated secondary antibody and DAPI using a commercially available mountant (SlowFade™, Molecular Probes, Eugene, OR, USA). Fluorescent images were collected with a laser scanning confocal microscope and Nikon NIS Elements software. Z-stacks (2 μm step size) were generated throughout the region of interest to generate optical dissectors for stereological sampling (400 μm dissector spacing, 14 μm dissector height). Z stacks were then transferred to Stereologer software (Stereology Resource Center Inc., Fl, USA) for sampling. Stereologer software was calibrated to actual XYZ measurements made during confocal image acquisition. Estimates of N for APC and DAPI were calculated using the formula, $N = 2 \times \sum \mathrm{I} \times 1/ssf \times 1/asf \times 1/\mathrm{hsf} \times 1/psd$. MBP-positive fiber length density (MBP-LD) was estimated using a computer generated spherical probe ("space balls") to score for isotropic fiber-probe interactions (Mouton et al., 2002). Total MBP length was divided by the volume of the region of interest to give a final length density (LD) estimate. Estimates for vacuole area volume fraction were generated also using the optical fractionator (k = 4) and an area fraction probe on H&E stained sections from the same brains as used for estimates of APC and DAPI. Vacuole area volume fraction was calculated using the formula, $\sum P_{obj}/\sum P_{ref} = A_{obj}/A_{ref} = V_{obj}/V_{ref}$, where P_{obj} = region points interacting with plaques, V_{obj} = region points interacting with the reference space, A = area, V = volume. Sampling integrity was monitored by maintaining a coefficient of sampling variance (CE) of <8% in order to identify true biological variance. Group means were compared between treatment and control groups using Student's *t*-test for unpaired means at the 95% confidence interval.

4.7. Analysis of motor function

Rotarod testing apparatus (MedAssociates Inc.) was used to assess motor function of all mice at 12 weeks of age. Testing took place over three consecutive days, with the first two days consisting of pre-trial training. Each day individual animals completed three consecutive runs with a 60 s delay between. On the third day, the average latency to fall of three runs was calculated for each animal. Significant differences in mean latency to fall were determined by Student's *t*-test for unpaired means. Daily activity patterns were measured using running wheels linked to wireless automated data collection software (Wheel Manager, MedAssociates Inc). Wheels were placed in cages with single mice for 7 consecutive days, and wheel turns recorded constantly. Data were analyzed using Wheel Analysis software (MedAssociates Inc.) and daily activity patterns used to calculate periodicity and confirm normal circadian rhythms.

Author contributions

JSF, PL, CJ, SJG, TJM, RJS conceived the experiments and wrote the article. IW, VM, LTB, DW, DD assisted with the acquisition and analysis of data.

Potential conflicts of interest

AAV Oligo patent (TM, SJG) applied for by UNC. RJS is the founder of AskBio and Bamboo Therapeutics. PL is scientific co-founder of Bamboo Therapeutics and scientific advisory Board member of Agilis Biotherapeutics.

Acknowledgements

This project was supported by Bamboo Therapeutics (15-0190 to PL) and partially by the NIH (STTR#R41G044890-01A1 to JS and NS088763-01A1 to PL) with additional support by the Canavan Research Illinois, the Ralph & Lois Silver Foundation, and Jacob's Cure. The development of the Olig001 capsid was supported by the Michel J. Fox Foundation to TJM. Indirect administrative support for SJG was provided by Research to Prevent Blindness to the UNC Department of Ophthalmology.

References

Ahmed, S.S., Li, H., Cao, C., Sikoglu, E.M., Denninger, A.R., Su, Q., Eaton, S., Liso Navarro, A.A., Xie, J., Szucs, S., Zhang, H., Moore, C., Kirschner, D.A., Seyfried, T.N., Flotte, T.R., Matalon, R., Gao, G., 2013. A single intravenous rAAV injection as late as P20 achieves efficacious and sustained CNS Gene therapy in Canavan mice. Mol. Ther. 21, 2136–2147.

Ahmed, S.S., Schattgen, S.A., Frakes, A.E., Sikoglu, E.M., Su, Q., Li, J., Hampton, T.G., Denninger, A.R., Kirschner, D.A., Kaspar, B., Matalon, R., Gao, G., 2016. rAAV Gene Therapy in a Canavan's Disease Mouse Model Reveals Immune Impairments and an Extended Pathology Beyond the Central Nervous System. Mol Ther.

Baslow, M.H., 2003. Brain *N*-acetylaspartate as a molecular water pump and its role in the etiology of Canavan disease: a mechanistic explanation. J. Mol. Neurosci. 21, 185–190.

Baslow, M.H., Suckow, R.F., Sapirstein, V., Hungund, B.L., 1999. Expression of aspartoacylase activity in cultured rat macroglial cells is limited to oligodendrocytes. J. Mol. Neurosci. 13, 47–53.

Bates, T.E., Strangward, M., Keelan, J., Davey, G.P., Munro, P.M., Clark, J.B., 1996. Inhibition of *N*-acetylaspartate production: implications for 1H MRS studies in vivo. Neuroreport 7, 1397–1400.

Burri, R., Steffen, C., Herschkowitz, N., 1991. *N*-acetyl-L-aspartate is a major source of acetyl groups for lipid synthesis during rat brain development. Dev. Neurosci. 13, 403–411.

Chakraborty, G., Mekala, P., Yahya, D., Wu, G., Ledeen, R.W., 2001. Intraneuronal *N*-acetylaspartate supplies acetyl groups for myelin lipid synthesis: evidence for myelin-associated aspartoacylase. J. Neurochem. 78, 736–745.

Clement, N., Grieger, J.C., 2016. Manufacturing of recombinant adeno-associated viral vectors for clinical trials. Mol Ther Methods Clin Dev. 3, 16002.

D'Adamo Jr., A.F., D'Adamo, A.P., 1968. Acetyl transport mechanisms in the nervous system. The oxoglutarate shunt and fatty acid synthesis in the developing rat brain. J. Neurochem. 15, 315–323.

De Stefano, N., Narayanan, S., Francis, G.S., Arnaoutelis, R., Tartaglia, M.C., Antel, J.P., Matthews, P.M., Arnold, D.L., 2001. Evidence of axonal damage in the early stages of multiple sclerosis and its relevance to disability. Arch. Neurol. 58, 65–70.

Dugas, J.C., Tai, Y.C., Speed, T.P., Ngai, J., Barres, B.A., 2006. Functional genomic analysis of oligodendrocyte differentiation. J. Neurosci. 26, 10967–10983.

Francis, J.S., Olariu, A., McPhee, S.W., Leone, P., 2006. Novel role for aspartoacylase in regulation of BDNF and timing of postnatal oligodendrogenesis. J. Neurosci. Res. 84, 151–169.

Francis, J.S., Strande, L., Pu, A., Leone, P., 2011. Endogenous aspartoacylase expression is responsive to glutamatergic activity in vitro and in vivo. Glia 59, 1435–1446.

Francis, J.S., Strande, L., Markov, V., Leone, P., 2012. Aspartoacylase supports oxidative energy metabolism during myelination. J. Cereb. Blood Flow Metab. 32, 1725–1736.

Francis, J.S., Markov, V., Leone, P., 2014. Dietary triheptanoin rescues oligodendrocyte loss, dysmyelination and motor function in the nur7 mouse model of Canavan disease. J. Inherit. Metab. Dis. 37, 369–381.

Funfschilling, U., Supplie, L.M., Mahad, D., Boretius, S., Saab, A.S., Edgar, J., Brinkmann, B.G., Kassmann, C.M., Tzvetanova, I.D., Mobius, W., Diaz, F., Meijer, D., Suter, U., Hamprecht, B., Sereda, M.W., Moraes, C.T., Frahm, J., Goebbels, S., Nave, K.A., 2012. Glycolytic oligodendrocytes maintain myelin and long-term axonal integrity. Nature 485, 517–521.

Gambetti, P., Mellman, W.J., Gonatas, N.K., 1969. Familial spongy degeneration of the central nervous system (Van Bogaert-Bertrand disease). An ultrastructural study. Acta Neuropathol. 12, 103–115.

Gray, S.J., Blake, B.L., Criswell, H.E., Nicolson, S.C., Samulski, R.J., McCown, T.J., Li, W., 2010. Directed evolution of a novel adeno-associated virus (AAV) vector that crosses the seizure-compromised blood-brain barrier (BBB). Mol. Ther. 18, 570–578.

Gray, S.J., Foti, S.B., Schwartz, J.W., Bachaboina, L., Taylor-Blake, B., Coleman, J., Ehlers, M.D., Zylka, M.J., McCown, T.J., Samulski, R.J., 2011. Optimizing promoters for recombinant adeno-associated virus-mediated gene expression in the peripheral and central nervous system using self-complementary vectors. Hum. Gene Ther. 22, 1143–1153.

Guo, F., Bannerman, P., Mills Ko, E., Miers, L., Xu, J., Burns, T., Li, S., Freeman, E., McDonough, J.A., Pleasure, D., 2015. Ablating *N*-acetylaspartate prevents leukodystrophy in a Canavan disease model. Ann. Neurol. 77, 884–888.

Hagenfeldt, L., Bollgren, I., Venizelos, N., 1987. *N*-acetylaspartic aciduria due to aspartoacylase deficiency–a new aetiology of childhood leukodystrophy. J. Inherit. Metab. Dis. 10, 135–141.

Hamm, R.J., Pike, B.R., O'Dell, D.M., Lyeth, B.G., Jenkins, L.W., 1994. The rotarod test: an evaluation of its effectiveness in assessing motor deficits following traumatic brain injury. J. Neurotrauma 11, 187–196.

Harris, J.J., Attwell, D., 2012. The energetics of CNS white matter. J. Neurosci. 32, 356–371.

Huang, W., Alexander, G.E., Chang, L., Shetty, H.U., Krasuski, J.S., Rapoport, S.I., Schapiro, M.B., 2001. Brain metabolite concentration and dementia severity in Alzheimer's disease: a (1)H MRS study. Neurology 57, 626–632.

Janson, C., McPhee, S., Bilaniuk, L., Haselgrove, J., Testaiuti, M., Freese, A., Wang, D.J., Shera, D., Hurh, P., Rupin, J., Saslow, E., Goldfarb, O., Goldberg, M., Larijani, G., Sharrar, W., Liouterman, L., Camp, A., Kolodny, E., Samulski, J., Leone, P., 2002. Clinical protocol. Gene therapy of Canavan disease: AAV-2 vector for neurosurgical delivery of aspartoacylase gene (ASPA) to the human brain. Hum. Gene Ther. 13, 1391–1412.

Janson, C.G., Kolodny, E.H., Zeng, B.J., Raghavan, S., Pastores, G., Torres, P., Assadi, M., McPhee, S., Goldfarb, O., Saslow, B., Freese, A., Wang, D.J., Bilaniuk, L., Shera, D., Leone, P., 2006a. Mild-onset presentation of Canavan's disease associated with novel G212A point mutation in aspartoacylase gene. Ann. Neurol. 59, 428–431.

Janson, C.G., McPhee, S.W., Francis, J., Shera, D., Assadi, M., Freese, A., Hurh, P., Haselgrove, J., Wang, D.J., Bilaniuk, L., Leone, P., 2006b. Natural history of Canavan disease revealed by proton magnetic resonance spectroscopy (1H-MRS) and diffusion-weighted MRI. Neuropediatrics 37, 209–221.

Klugmann, M., Leichtlein, C.B., Symes, C.W., Serikawa, T., Young, D., During, M.J., 2005. Restoration of aspartoacylase activity in CNS neurons does not ameliorate motor deficits and demyelination in a model of Canavan disease. Mol. Ther. 11, 745–753.

Kuhn, P.L., Petroulakis, E., Zazanis, G.A., McKinnon, R.D., 1995. Motor function analysis of myelin mutant mice using a rotarod. Int. J. Dev. Neurosci. 13, 715–722.

Lazzarino, G., Amorini, A.M., Fazzina, G., Vagnozzi, R., Signoretti, S., Donzelli, S., Di Stasio, E., Giardina, B., Tavazzi, B., 2003. Single-sample preparation for simultaneous cellular redox and energy state determination. Anal. Biochem. 322, 51–59.

Leone, P., Janson, C.G., Bilaniuk, L., Wang, Z., Sorgi, F., Huang, L., Matalon, R., Kaul, R., Zeng, Z., Freese, A., McPhee, S.W., Mee, E., During, M.J., 2000. Aspartoacylase gene transfer to the mammalian central nervous system with therapeutic implications for Canavan disease. Ann. Neurol. 48, 27–38.

Leone, P., Shera, D., McPhee, S.W., Francis, J.S., Kolodny, E.H., Bilaniuk, L.T., Wang, D.J., Assadi, M., Goldfarb, O., Goldman, H.W., Freese, A., Young, D., During, M.J., Samulski, R.J., Janson, C.G., 2012. Long-term follow-up after gene therapy for canavan disease. Sci. Transl. Med. (4:165ra163).

Madhavarao, C.N., Moffett, J.R., Moore, R.A., Viola, R.E., Namboodiri, M.A., Jacobowitz, D.M., 2004. Immunohistochemical localization of aspartoacylase in the rat central nervous system. J. Comp. Neurol. 472, 318–329.

Madhavarao, C.N., Arun, P., Moffett, J.R., Szucs, S., Surendran, S., Matalon, R., Garbern, J., Hristova, D., Johnson, A., Jiang, W., Namboodiri, M.A., 2005. Defective *N*-acetylaspartate catabolism reduces brain acetate levels and myelin lipid synthesis in Canavan's disease. Proc. Natl. Acad. Sci. U. S. A. 102, 5221–5226.

Maier, H., Wang-Eckhardt, L., Hartmann, D., Gieselmann, V., Eckhardt, M., 2015. N-acetylaspartate synthase deficiency corrects the myelin phenotype in a Canavan disease mouse model but does not affect survival time. J. Neurosci. 35, 14501–14516.

Martin, E., Capone, A., Schneider, J., Hennig, J., Thiel, T., 2001. Absence of *N*-acetylaspartate in the human brain: impact on neurospectroscopy? Ann. Neurol. 49, 518–521.

Matalon, R., Surendran, S., Rady, P.L., Quast, M.J., Campbell, G.A., Matalon, K.M., Tyring, S.K., Wei, J., Peden, C.S., Ezell, E.L., Muzyczka, N., Mandel, R.J., 2003. Adeno-associated virus-mediated aspartoacylase gene transfer to the brain of knockout mouse for canavan disease. Mol. Ther. 7, 580–587.

McKenna, M.C., Waagepetersen, H.S., Schousboe, A., Sonnewald, U., 2006. Neuronal and astrocytic shuttle mechanisms for cytosolic-mitochondrial transfer of reducing equivalents: current evidence and pharmacological tools. Biochem. Pharmacol. 71, 399–407.

McPhee, S.W., Francis, J., Janson, C.G., Serikawa, T., Hyland, K., Ong, E.O., Raghavan, S.S., Freese, A., Leone, P., 2005. Effects of AAV-2-mediated aspartoacylase gene transfer in the tremor rat model of Canavan disease. Brain Res. Mol. Brain Res. 135, 112–121.

McPhee, S.W., Janson, C.G., Li, C., Samulski, R.J., Camp, A.S., Francis, J., Shera, D., Liouterman, L., Feely, M., Freese, A., Leone, P., 2006. Immune responses to AAV in a phase I study for Canavan disease. The Journal of Gene Medicine. 8, 577–588.

Mehta, V., Namboodiri, M.A., 1995. *N*-acetylaspartate as an acetyl source in the nervous system. Brain Res. Mol. Brain Res. 31, 151–157.

Moffett, J.R., Ross, B., Arun, P., Madhavarao, C.N., Namboodiri, A.M., 2007. *N*-acetylaspartate in the CNS: from neurodiagnostics to neurobiology. Prog. Neurobiol. 81, 89–131.

Moreno, A., Ross, B.D., Bluml, S., 2001. Direct determination of the *N*-acetyl-L-aspartate synthesis rate in the human brain by (13)C MRS and [1-(13)C]glucose infusion. J. Neurochem. 77, 347–350.

Mouton, P.R., Gokhale, A.M., Ward, N.L., West, M.J., 2002. Stereological length estimation using spherical probes. J. Microsc. 206, 54–64.

Rinholm, J.E., Hamilton, N.B., Kessaris, N., Richardson, W.D., Bergersen, L.H., Attwell, D., 2011. Regulation of oligodendrocyte development and myelination by glucose and lactate. J. Neurosci. 31, 538–548.

Sauvageot, C.M., Stiles, C.D., 2002. Molecular mechanisms controlling cortical gliogenesis. Curr. Opin. Neurobiol. 12, 244–249.

Sturrock, A., Laule, C., Decolongon, J., Dar Santos, R., Coleman, A.J., Creighton, S., Bechtel, N., Reilmann, R., Hayden, M.R., Tabrizi, S.J., Mackay, A.L., Leavitt, B.R., 2010. Magnetic resonance spectroscopy biomarkers in premanifest and early Huntington disease. Neurology 75, 1702–1710.

Taylor, D.L., Davies, S.E., Obrenovitch, T.P., Doheny, M.H., Patsalos, P.N., Clark, J.B., Symon, L., 1995. Investigation into the role of *N*-acetylaspartate in cerebral osmoregulation. J. Neurochem. 65, 275–281.

Traka, M., Wollmann, R.L., Cerda, S.R., Dugas, J., Barres, B.A., Popko, B., 2008. Nur7 is a nonsense mutation in the mouse aspartoacylase gene that causes spongy degeneration of the CNS. J. Neurosci. 28, 11537–11549.

Wiame, E., Tyteca, D., Pierrot, N., Collard, F., Amyere, M., Noel, G., Desmedt, J., Nassogne, M.C., Vikkula, M., Octave, J.N., Vincent, M.F., Courtoy, P.J., Boltshauser, E., van Schaftingen, E., 2010. Molecular identification of aspartate *N*-acetyltransferase and its mutation in hypoacetylaspartia. Biochem. J. 425, 127–136.

Zhang, Y., Chen, K., Sloan, S.A., Bennett, M.L., Scholze, A.R., O'Keeffe, S., Phatnani, H.P., Guarnieri, P., Caneda, C., Ruderisch, N., Deng, S., Liddelow, S.A., Zhang, C., Daneman, R., Maniatis, T., Barres, B.A., Wu, J.Q., 2014. An RNA-sequencing transcriptome and splicing database of glia, neurons, and vascular cells of the cerebral cortex. J. Neurosci. 34, 11929–11947.